Journal of Alloys and Compounds 990 (2024) 174446

Contents lists available at ScienceDirect

Journal of Alloys and Compounds

journal homepage: www.elsevier.com/locate/jalcom

Efficient and environmentally friendly separation and recycling of cathode materials and current collectors for lithium-ion batteries by fast Joule heating

Chengxiang Li [a,*], Pengfei Kou [a], Hong Wen [a], Yan Zhou [a,b], Xuzhao Gao [a], Yan Mi [a]

[a] School of Electrical Engineering, Chongqing University, Chongqing 400030, China
[b] School of Electronics and IoT, Chongqing College of Electronic Engineering, Chongqing 401331, China

ARTICLE INFO

Keywords:
Spent lithium-ion batteries
Cathode materials
Current collectors
Fast joule heating
Recycling
Environmentally friendly

ABSTRACT

Spent Li-ion batteries(LIBs) cathodes possess high recycling value. To improve subsequent recovery efficiency and product purity, separating the cathode materials from the aluminum foil is critical. However, traditional separation methods are characterized by high energy consumption, low recycling efficiency, and environmental pollution. This research presents a novel method that involves injecting Joule heat directly into the aluminum foil in the air, resulting in the melting and slight thermal decomposition of the PVDF binder, which reduces its adhesive properties. Owing to the difference in thermal expansion coefficients between the binder and aluminum foil, an instantaneous thermal stress was generated at the interface of the cathode materials and aluminum foil, resulting in a peeling force. This method enabled a rapid and efficient separation of lithium iron phosphate (LFP) and ternary Li-ion (NCM) battery cathode materials. The optimal separation conditions, separation mechanism, and properties of the recovered products were investigated thoroughly using high-speed camera imaging, temperature rise calculations, and microscopic characterization. This chemical-free method avoids the generation of wastewater and gas emissions. Under optimal experimental parameters, the separation efficiency and purity of cathode material reached 99 % and 99.7 %, respectively. Additionally, this method preserves both the structural integrity of the aluminum foil and the crystalline structure of the cathode materials, offering a new pathway for sustainable recycling of end-of-life LIBs.

1. Introduction

Lithium-ion batteries (LIBs), characterized by high operating voltage, wide operating temperature range, high energy density, and no memory effect, are widely used in various fields such as mobile devices, grid energy storage, and electric vehicles[1–4].

However, the finite lifespan of LIBs presents significant challenges. It has been predicted that more than 11 million tonnes of spent LIBs will be generated globally between 2017 and 2030, posing significant environmental and resource challenges[5,6]. These spent batteries contain numerous high-value but toxic and non-renewable resources, including metals such as lithium, cobalt, nickel, manganese, and aluminum. The improper recycling of these batteries not only results in the wastage of valuable resources but also poses considerable threats to both the environment and human health[7].

In the recycling of LIBs, cathode materials are the primary focus, as they contain the majority of the valuable metals in these batteries and account for approximately 30–40 % of the manufacturing cost[8]. The cathode of a LIB is composed of a sandwich structure where the cathode active material is tightly bonded to aluminum foil using adhesives such as polyvinylidene fluoride (PVDF)[9]. Ensuring complete separation of cathode active materials from the aluminum foil is critical for the efficiency of subsequent hydrometallurgical leaching to recover valuable elements from spent LIBs [10]. Due to the strong adhesive bond between the cathode material and the aluminum foil, their separation and subsequent recycling become difficult[11]. Consequently, achieving selective separation of aluminum foil and cathode materials presents a significant challenge.

Global researchers have explored numerous methods to separate the aluminum foil from the cathode materials in LIBs. These methods involve reducing the adhesive properties of PVDF, applying mechanical peeling force, and the combination of these techniques. The primary methods are as follows:

* Corresponding author.
E-mail address: lichengxiang@cqu.edu.cn (C. Li).

https://doi.org/10.1016/j.jallcom.2024.174446
Received 16 February 2024; Received in revised form 3 April 2024; Accepted 7 April 2024
Available online 9 April 2024
0925-8388/© 2024 Elsevier B.V. All rights reserved.

1.1. Organic solvent method

Currently, the organic binder in cathode materials is mainly PVDF. According to the "like dissolves like" principle, N-methylpyrrolidone (NMP) is used as the organic solvent to dissolve PVDF[12–15]. Xin et al. immersed cathode sheets in an NMP solution for 1–2 hours to allow the cathode materials to detach from the aluminum foil[16]. Following dissolution, the pure cathode materials were obtained by filtration. However, NMP is an expensive solvent, accounting for 10 % of the electrode production cost, and is also toxic[17].

1.2. Aluminum foil dissolution method

In this approach, aluminum foil is dissolved in a NaOH solution, followed by filtration and drying processes to recover cathode materials. Although straightforward and effective, this method results in the production of significant toxic waste liquids[18,19].

1.3. Pyrolysis method

This method entails the thermal treatment of cathode materials at high temperatures (500–600°C) to decompose PVDF and diminish its adhesive properties. Subsequently, methods, including mechanical vibration screening, high-speed mechanical rotation shredding, and high-speed gas jet separation, are employed to obtain the cathode materials [20–22]. However, this approach is energy-intensive, and the thermal decomposition of PVDF leads to the generation of fluorides, which are detrimental to the environment and highly toxic to humans[23].

1.4. Mechanical shredding method

This method utilizes a shearing force on the cathode material and aluminum foil, effectively pulverizing the cathode material and facilitating its separation from the foil. Although efficient in industrial applications, this method frequently leads to over-crushing of the aluminum foil, thereby resulting in high aluminum content in the cathode materials (yielding a recovery efficiency of only 70–80 %), which poses significant challenges in subsequent separation and purification[24].

Recently, researchers had innovative methods to tackle the challenge of separating cathode materials from aluminum foil in LIBs. These methods include the cryogenic grinding technique, low-temperature molten salt system, and electromagnetic heating separation technology[25–27].

Pulsed power technology is an electrophysical technique that compresses energy and rapidly releases it onto a load. According to reports, pulsed power technology—which instantaneously generates plasma, shock waves, or significant thermal energy—is used for the separation and recovery of various materials. Applications include separating aggregates in waste concrete, recovering metallic silver from discarded photovoltaic panels, extracting precious metals from waste circuit boards, and producing graphene[28–33]. The method is characterized by its high selectivity in separation and its ability to yield controllable separation results. Recently, scientists have proposed the use of a pulsed power system in water to fracture and separate LIBs or their cathode sheets[34–36]. In this approach, shock waves generated by underwater discharge provide the necessary force for fragmentation or peeling. Compared to mechanical shredding, this approach offers higher selectivity but requires high working voltages (several tens of kilovolts), necessitating advanced equipment standards. Furthermore, it requires 1500 to 2500 discharges to break the battery. Although this method did not use additional chemicals, the process generated wastewater, thereby increasing the complexity and cost of the operation.

A technological approach to separating cathode materials from aluminum foil in LIBs involved applying heat or a peeling force to the cathode materials, similar to the effects of pulsed power technology. For instance, Wang demonstrated this process by continuously stirring a LIB cathode sheet in an $AlCl_3$-NaCl molten salt system at 160°C using a glass rod for 20 minutes, resulting in the separation of the cathode material from the aluminum foil[26]. The principle behind this separation is that melting the PVDF deactivates it, significantly reducing its adhesive properties. Additionally, many researchers have heated the cathode material to 500–600°C for 0.5–1 hour to completely decompose PVDF thermally, followed by employing vibrating screens, ultrasonic vibration, or mechanical crushing to apply additional peeling force for the separation[22,37,38].

This study focused on a crucial step in the recycling process of LIBs: separating the cathode materials from the aluminum foil. Current methods for this process suffer from environmental pollution, high energy consumption, and low separation efficiency. To address these challenges, a pulsed power system was devised to separate the cathode materials from the aluminum foil in LIBs. This study entailed the instant injection of significant heat directly into the aluminum foil of the cathode sheet, significantly reducing the adhesive properties between the aluminum foil and the cathode materials. Owing to the multilayer structure of lithium-ion battery cathode materials, rapid Joule heating could generate thermal stress at the interface, offering the necessary force for peeling without relying on shock waves. In multilayer materials, a thermal mismatch can occur during heating and cooling due to temperature variations and differences in thermal expansion coefficients among layers. This phenomenon may lead to the formation of cracks or the separation of layers within the material. This type of failure has been observed in thermal barrier coatings, chip packaging, and battery electrode materials[39–44]. The study confirmed the feasibility of this method, investigated the separation mechanism and behavior, and identified key parameters affecting the efficiency of cathode material delamination, such as charging voltage and current pulse width. Material testing was performed on the separated products. This method offers numerous advantages: rapid processing, high efficiency, low energy consumption, no use of chemical reagents, and no generation of exhaust gases or wastewater, highlighting its potential for the recovery and reuse of cathode materials.

2. Materials and methods

2.1. Experimental materials

In this study, depleted LFP and NCM batteries were used as subjects in the separation and recovery experiments. To prevent short-circuiting and self-ignition, the spent lithium batteries were initially discharged in a 5.0 wt% sodium chloride solution for 48 hours, then air-dried for 24 hours. The batteries were manually disassembled to remove the casing, separator, and anode sheets. The cells were then washed with DMC solvent to remove the electrolyte. Subsequently, the cathode sheets were cut into 200 mm×20 mm dimensions for use as samples in the experiments. Each sample's weight was measured using an electronic balance: 1.115 g for the LFP cathode sheet and 1.058 g for the NCM cathode sheet. As illustrated in Fig. 1(a)-(d), the SEM images and structure schematics of the LFP and NCM cathode sheets reveal that the cathode current collector is composed of aluminum foil approximately 16 μm thick. The cathode material, which includes a mixture of active materials ($LiFePO_4$ or $Li(Ni_{0.5}Co_{0.2}Mn_{0.3})O_2$) and minor quantities of acetylene black and PVDF, was coated on both sides of the current collector. For NCM cathode sheets, the single-sided coating thickness was approximately 48 μm, while it was about 74 μm for LFP cathode sheets.

Since the distribution, bond strength, and mechanism of action of PVDF in different types of cathode sheets are significantly different [23]. Consequently, even with the use of the same separation technology, the separation results could vary significantly among different LIB cathode materials. Therefore, this study conducted experiments with two different types of LIB cathode sheets.

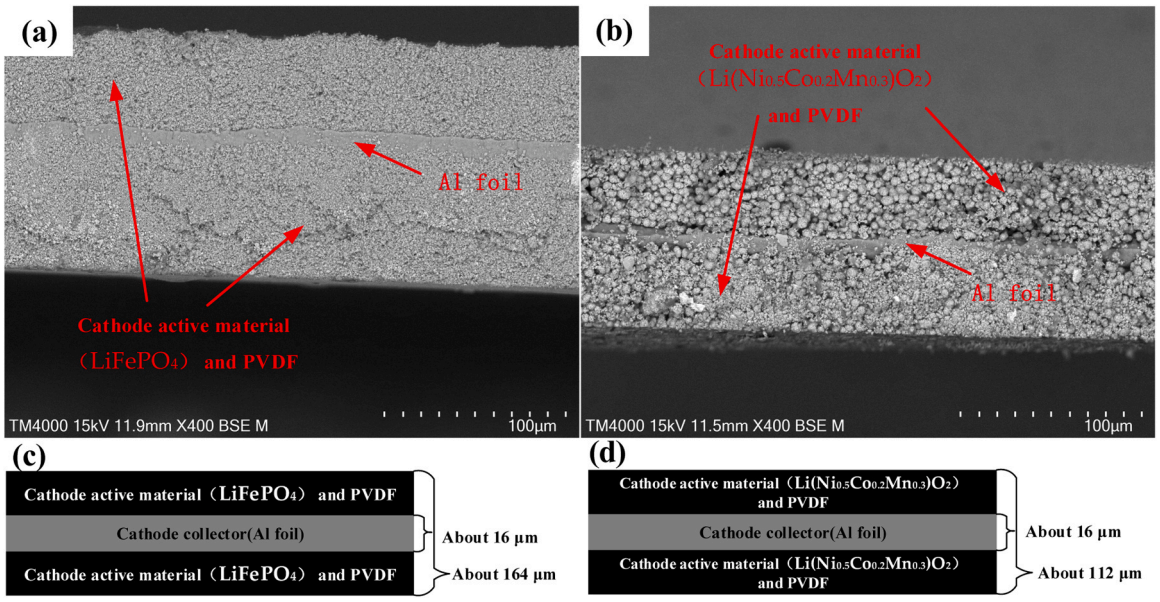

Fig. 1. **(a)** SEM image of LFP cathode sheet cross-section; **(b)** SEM image of NCM cathode sheet cross-section; **(c)** Structure schematic of LFP cathode sheet cross-section; **(d)** Structure schematic of NCM cathode sheet cross-section.

2.2. Pulse discharge Joule heat separation system and high-speed imaging system

Fig. 2 illustrates the experimental circuit and high-speed imaging device. As depicted in Fig. 2, the circuit structure of the pulse-discharge thermal stress separation device consists of a charging circuit and a discharging circuit. In the charging circuit, a high voltage direct current (HVDC) power supply charged the capacitor. A vacuum relay, serving as the charging switch, allowed the HVDC supply to charge the capacitor when open. Upon reaching the desired voltage, the vacuum relay was closed, isolating the discharge circuit from the charging circuit during discharge. The capacitor used was a 100 μF/5 kV film type. In the discharge circuit, the switch was a pulse thyristor (5.3 kV/130 kA) controlled by a 30 V/1 μs trigger source. A freewheeling diode (6.5 kV/16.5 kA) connected in parallel with the capacitor protected the thyristor switch from overvoltage during turn-off and provided a current path when the capacitor voltage was negative. The LIB cathode sheet, acting as the load, was clamped using copper electrodes. During the experiment, the capacitor's working voltage was measured with a high voltage probe (Tektronix P6015A), the discharge current with a Rogowski coil (CP9302L) and an integrator, and voltage and current waveforms were captured using an oscilloscope (Tektronix MDO3024).

To investigate the separation mechanism of aluminum foil and cathode materials, a high-speed camera was used to record the cathode sheet's separation motion during discharge. Additionally, a high-speed optical imaging platform, as depicted on the right side of Fig. 2, was constructed. The observation platform comprised an auxiliary light using a DC non-flickering LED (200 W) and a high-speed camera (SSZN SH6) with a fixed-focus lens (SIGMA 105 mm 1:2.8). As the capacitor discharged, the oscilloscope recorded the voltage and current waveforms and simultaneously sent a trigger signal to the high-speed camera, initiating image capture.

2.3. Experimental procedure

To verify the separation of LIB cathode materials at different voltages, NCM and LFP samples, measuring 200 mm×20 mm, were clamped between two copper electrode plates with an electrode distance of 175 mm between the electrodes. The experiments were conducted at charging voltages ranging from 2.0 kV to 3.5 kV, in increments of

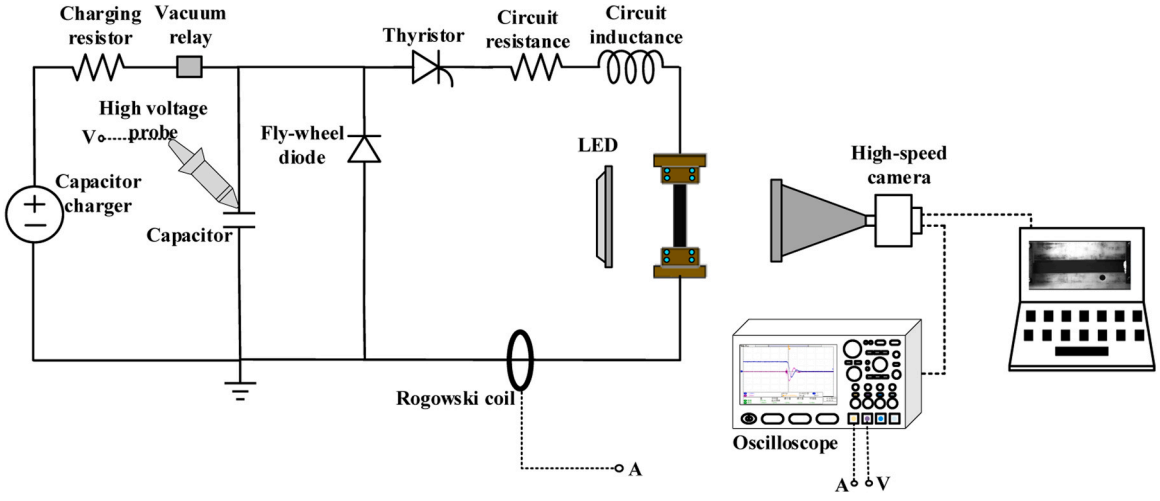

Fig. 2. Experimental circuit and high-speed imaging system.

0.25 kV, with a charging capacitance of 100 μF.

The separation rate of the cathode material was calculated as follows:

$$\eta\left(\%\right) = \frac{W_1}{(W_2 - W_0)} \times 100\%, \quad (1)$$

where W_1 represents the mass of the cathode materials obtained after separation, W_2 is the mass of the cathode sheet before the experiment, and W_0 is the theoretical mass of the aluminum foil in the cathode sheet. W_0 could be obtained from the battery manufacturer or calculated based on the density and dimensions of the aluminum foil. In the case of a 20 mm×200 mm cathode sheet sample, the mass of the aluminum foil (W_0) was 0.1728 g. W_1 represents the mass of the cathode materials actually obtained through separation, and (W_2-W_0) represents the theoretical mass of the cathode materials.

2.4. Material characterisation

The sample was subjected to microwave-assisted acid dissolution using a mixture of perchloric acid, concentrated nitric acid, and concentrated hydrochloric acid (in a ratio of 1:3:1) at a solid-liquid ratio of 1:100 g/mL and heated to 280°C for 60 minutes. Following acid dissolution, the elemental content in the cathode materials, both pre-separation and post-separation, was analyzed using an Inductively Coupled Plasma Optical Emission Spectrometer (ICP-OES, PE Avio 200). Microstructural and elemental analysis of the cathode materials was conducted using an Environmental Scanning Electron Microscope (ESEM, Quattro S) and a Desktop Scanning Electron Microscope (SEM, TM-4000 Plus). Phase changes in the cathode materials, both before and after separation, were evaluated using an X-ray Diffractometer (XRD, Bruker D8 Advance) in a wide-angle diffraction mode (10–90°) at a scan rate of 8°/min.

3. Results and discussion

3.1. Separation of cathode materials at different voltages

The separation conditions of the LFP battery cathode samples after pulse discharge treatment at different charging voltages are shown in Fig. 3(a)-(c). At a charging voltage of 2.0 kV, there was no observable separation between the LFP cathode material and the aluminum foil. Fig. 3(a) illustrates that at 2.5 kV, separation of the cathode material from the aluminum foil occurred only at the edges of the cathode sheet, indicating initiation of separation from the edges. Fig. 3(b) shows that at 3.0 kV, there was complete separation between the cathode material and the aluminum foil, with both components maintaining their structural integrity. Upon achieving a charging voltage of 3 kV, the recovered aluminum foil was washed, dried, and weighed using an electronic balance, registering a mass of 0.170 g. Following simple sieving, the separated products were readily processed for subsequent hydrometallurgical steps.

Unlike cathode material recovery, the recycling of aluminum foil often goes unnoticed. According to a report by Goodfellow in August 2021, the costs for aluminum and copper foil were approximately $130 and $640 per square meter, respectively, for a 20 μm thickness and a purity of over 99 %[45]. Additionally, recycling aluminum in the manufacturing process of electric vehicles can potentially reduce energy consumption by 33 %[45]. Therefore, recycling aluminum foil is essential, and preserving its structural integrity during the separation process is of significant importance. Minor wrinkling was observed at the radial edges of the aluminum foil, in contrast to the central surface morphology. This phenomenon is attributed to the high frequency of the electrical pulses applied and the skin effect, where the current primarily flows through the edges of the aluminum foil, causing higher temperatures at these locations. This also explains why the separation of the cathode material from the aluminum foil starts at the edges at a charging voltage of 2.5 kV. At a charging voltage of 3.5 kV, the aluminum foil and the cathode material achieved nearly complete separation. Under the influence of the electromagnetic force, the aluminum foil contracted into a wire-like shape, leaving residual aluminum at the edges of the cathode material. This contraction was caused by the elevated temperatures at the edges of the foil during the pulse discharge treatment. The temperatures reached aluminum's melting point, resulting in some aluminum residue on the cathode material. Eqs. (2) and (3) demonstrate the electromagnetic force and radial pressure that cause the inward contraction of the aluminum foil.

$$F(t) = \frac{\mu_0 I(t)^2 b}{2\pi a}, \quad (2)$$

$$P(t) = \frac{\mu_0 I(t)^2}{2\pi a \tau}, \quad (3)$$

In the formula, μ_0 represented the vacuum permeability, $4\pi\times10^{-7}$ N/A^2, where a and b were the width and length of the aluminum foil,

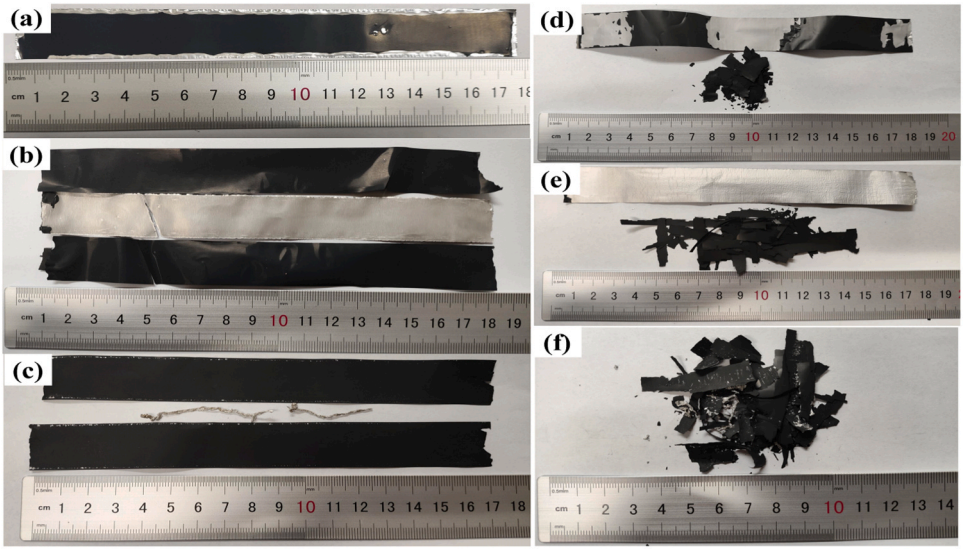

Fig. 3. Cathode material and aluminum foil after electric pulse treatment **(a)** at a charging voltage of 2.5 kV for LFP batteries; **(b)** at 3.0 kV for LFP batteries; **(c)** at 3.5 kV for LFP batteries; **(d)** at 2.5 kV for NCM batteries; **(e)** at 3.0 kV for NCM batteries; **(f)** at 3.5 kV for NCM batteries.

respectively. Calculations showed that at a charging voltage of 3.5 kV, the maximum peak current was approximately 20.1 kA, resulting in a maximum radial pressure on the aluminum foil of approximately 250 MPa.

The separation of the NCM battery cathode samples after pulse discharge treatment at different charging voltages is shown in Fig. 3(d)-(f). At 2.0 kV, there was no observable separation between the cathode material and the aluminum foil. At 2.5 kV, partial separation between the cathode material and the aluminum foil was observed, showing a higher separation rate compared to LFP batteries. Curvature in the unseparated areas of the cathode sheet was noted, attributed to residual thermal stress caused by differing material properties of the aluminum foil and cathode material during heating and cooling, leading to warping [46,47]. At 3.0 kV, complete separation between the cathode material and aluminum foil was achieved; unlike the LFP cathode materials, the NCM cathode materials became fragmented. At 3.5 kV, essential separation of the aluminum foil and cathode material was achieved; however, the aluminum foil fractured due to excessive Joule heat, resulting in some parts melting and adhering to the cathode material. Fig. 4 illustrates the relationship between the peel-off efficiency of the cathode material coating and the aluminum foil in both LFP and NCM batteries at various charging voltages.

3.2. High-speed cameras capture the separation process

Fig. 5(a) depicts the separation behavior of a 200 mm×20 mm LFP battery cathode sheet, as captured by a high-speed camera at a charging voltage of 3.0 kV. Discharge began at 22 μs, accompanied by the emergence of an arc plasma on the positive side of the copper clamp electrode. With the development of the arc plasma, the current swiftly passed through the aluminum foil, leading to substantial Joule heat deposition. The separation began at the specimen's edge near the negative side of the copper clamp electrode and progressively moved towards the positive side, where the arc transformed into a jet. At 11782 μs, wrinkles appeared on the sample surface near the positive side of the holding electrode, initiating separation; by 23836 μs, complete separation of the cathode material from the aluminum foil occurred.

Fig. 5(b) illustrates the separation behavior of a 200 mm×20 mm NCM battery cathode sheet, recorded at a charging voltage of 3.0 kV. The separation behavior of NCM batteries is markedly different from that of LFP batteries. Upon discharge initiation at 20 μs, an arc plasma emerged on the positive side of the copper clamp electrode. At 130 μs, the arc plasma expanded to both the positive and negative sides of the clamp electrode, with horizontal cracks appearing in the NCM battery's cathode material. By 970 μs, the cathode material cracks widened, forming a reticulated structure, leading to its detachment from the aluminum foil, as the arc plasma evolved into a jet. Finally, by 3970 μs, the cathode material cracked into strips and separated from the aluminum foil, which retained its structural integrity.

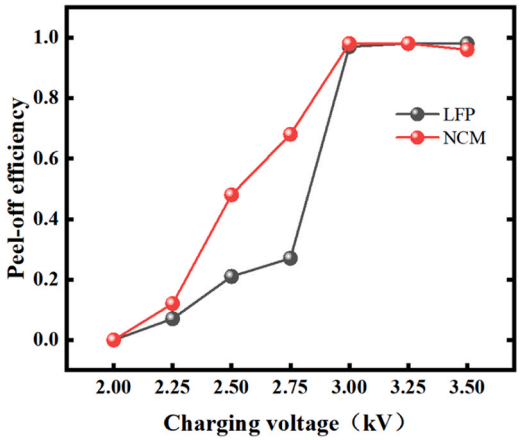

Fig. 4. Peel-off efficiency at different charging voltages.

The differing separation behavior between NCM and LFP battery cathode materials is primarily attributed to the varied distribution of PVDF in these materials[23]. In LFP batteries, PVDF predominantly coats the surface of $LiFePO_4$ particles, while in NCM batteries, it is uniformly distributed between the aluminum foil and $Li(Ni_xCo_yMn_{1-x-y})O_2$ particles. This leads to a stronger interaction between PVDF and $LiFePO_4$ particles in LFP batteries compared to that between PVDF and aluminum foil. Conversely, in NCM batteries, the interaction between PVDF and $Li(Ni_xCo_yMn_{1-x-y})O_2$ particles is less robust than with aluminum foil. Consequently, NCM battery cathode materials are more susceptible to cracking and breakage during the separation process.

3.3. Discharge current and temperature rise

Fig. 6(a)-(c) depict the capacitor voltage and load current waveforms at charging voltages of 2.5 kV, 3.0 kV, and 3.5 kV, with corresponding peak currents of 15.1 kA, 18.2 kA, and 20.1 kA, and a current pulse width of about 40 μs.

Given the extremely short discharge time, heat transfer from the aluminum foil to other materials can be neglected. Assuming uniform current distribution across the aluminum foil, the temperature rise during the discharge process can be approximated using the following thermal equilibrium formula:

$$Q_{in} = m_{Al}c_{Al}\Delta T, \tag{4}$$

where Q_{in} represented the Joule heat input into the aluminum foil, m_{Al} was the mass of the aluminum foil, c_{Al} was the specific heat capacity of the aluminum foil, and ΔT was the change in temperature of the aluminum foil.

$$Q_{in} = R_{Al}I^2\Delta t, \tag{5}$$

where,R_{Al} denoted the resistance of the aluminum foil, I was the current passing through the aluminum foil, Δt was the duration of the current flow through the aluminum foil.

$$R_{Al} = \rho_{Al}L_{Al}/(W_{Al}\tau_{Al}), \tag{6}$$

$$\Delta T = \left(\rho_{Al}L_{Al}I^2\Delta t\right)/\left(W_{Al}\tau_{Al}m_{Al}c_{Al}\right), \tag{7}$$

In the equation, ρ_{Al} represented the resistivity of the aluminum foil, L_{Al} was the length of the aluminum foil, W_{Al} was the width of the aluminum foil, and τ_{Al} was the thickness of the aluminum foil.

According to calculations using Eqs. (4), (5), (6), and (7), during pulse treatment at charging voltages of 2.5 kV, 3.0 kV, and 3.5 kV, the aluminum foil reached peak temperatures of 646 K, 757 K, and 851 K, respectively.

Fig. 6(d) shows that the temperature of the aluminum foil never exceeded its melting point of 933 K. However, during experiments at a charging voltage of 3.5 kV, the aluminum foil experienced fragmentation, with some parts melting and adhering to the cathode material. This was due to the high frequency of applied electrical pulses, which caused a higher current density at the edges of the aluminum foil compared to the center, making it more susceptible to erosion by the arc plasma near the electrodes. Consequently, the actual temperature of the aluminum foil may have been slightly higher than the calculated values shown in Fig. 6(d).

At charging voltages of 2.5 kV and 3.0 kV, the temperature of the aluminum foil remained significantly lower than its melting point, enabling it to retain its structural integrity after discharge treatment, as shown in Fig. 3. Experimental results in Fig. 3 showed that the temperature increase caused by the 3.0 kV discharge was sufficient to separate the cathode material from the aluminum foil, but this was not the case for the 2.5 kV and 2.0 kV discharges. Wang reported that melting deactivates PVDF, significantly reducing its adhesive properties

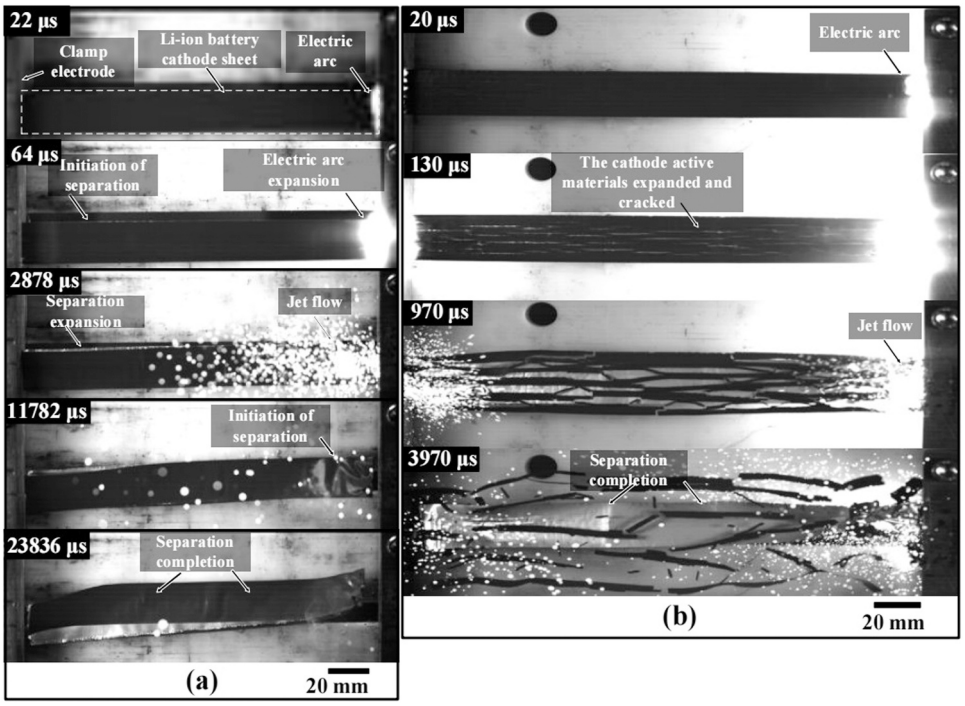

Fig. 5. Images of cathode materials separation behaviour at a charging voltage of 3.0 kV **(a)** LFP battery; **(b)** NCM battery.

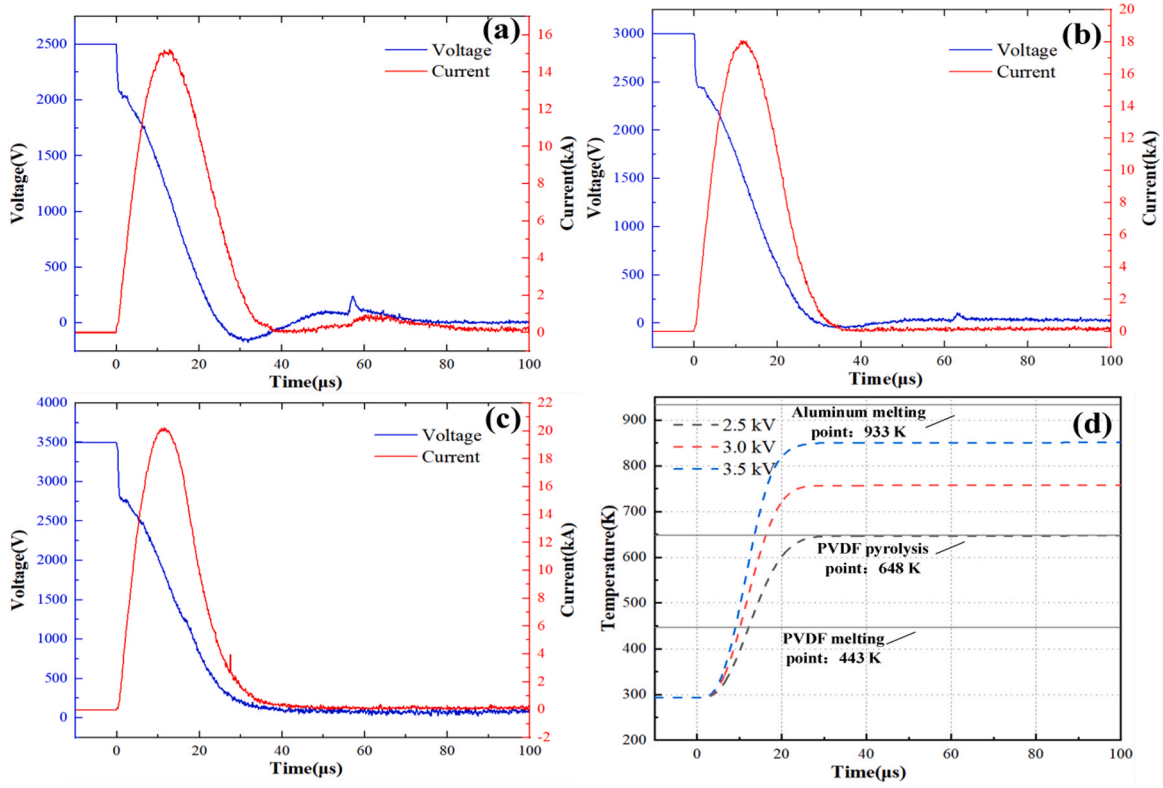

Fig. 6. **(a)** Capacitor voltage and load current curves at a charging voltage of 2.5 kV; **(b)** Capacitor voltage and load current curves at a charging voltage of 3.0 kV; **(c)** Capacitor voltage and load current curves at a charging voltage of 3.5 kV; **(d)** Temperature rise curves of aluminum foil during discharge at different charging voltages.

[26]. Zhang's findings indicate that the direct thermal decomposition of PVDF in cathode sheets requires a temperature of 500°C[37]. Complete thermal decomposition of PVDF typically occurs at 600°C over 30 minutes[48]. Therefore, during the pulse treatment, as the aluminum foil's instantaneous maximum surface temperature exceeded PVDF's melting point (443 K) and thermal decomposition temperature (648 K), the adhesive at the bonding interface melted and potentially partially decomposed, significantly reducing its adhesive properties[49]. While

simple heating can significantly reduce PVDF's adhesive properties, additional peeling forces like ultrasonic vibration or mechanical crushing are still needed to separate the cathode material from the aluminum foil post-heating[22,37,38]. Given that aluminum, being a metal, has a coefficient of thermal expansion (CTE) of $23\times10^{-6}\cdot k^{-1}$, and PVDF, as an organic material, has a CTE of $127.8\times10^{-6}\cdot k^{-1}$ - 5.6 times that of aluminum[50,51]. A mismatch in the coefficients of thermal expansion in a sandwich structure such as the Li-ion battery cathode sheet will lead to thermal mismatch during heating and cooling, resulting in peeling and shear stresses at the interface, ultimately leading to cracking and complete separation. The linear thermal expansion due to temperature changes in the materials was expressed by Eq. (8):

$$\Delta L = \alpha \Delta T L, \tag{8}$$

where, ΔL represented the amount of linear thermal expansion, α was the thermal expansion coefficient, ΔT was the temperature change, and L was the initial length.

3.4. Effect of pulse width (heating rate)

To examine the impact of electrical pulse heating duration on the separation efficiency of cathode materials from aluminum foil in LIBs, electric pulses with widths of approximately 40 μs, 400 μs, and 5000 μs were applied to 200 mm × 20 mm LFP battery cathode sheets. Figs. 6(b), 7(a), and 7(b) display the current and voltage waveforms for these pulses, respectively. To deliver the same total energy to the load, different pulse widths were set according to the temperature conditions necessary for complete cathode material separation from the aluminum foil, as detailed in Section 3.2, achieving an approximate temperature rise of 750 K in the aluminum foil. Experimental results showed that perfect separation of the cathode material from the aluminum foil occurred after a 40 μs pulse treatment, whereas no separation was observed with 400 μs and 5000 μs pulses.

The cross-sectional morphology of the cathode sheet samples after treatment with different pulse widths was characterised by SEM, as shown in Fig. 8. It was observed that shorter electrical pulses were able to heat the aluminum foil to the specified temperature in a shorter time, inducing greater thermal stress effects at the interface between the cathode material and the aluminum foil. This resulted in the formation of wider cracks, which further developed to achieve complete separation of the cathode material from the aluminum foil. Conversely, longer pulses resulted in lesser thermal stress at the interface, leading to narrower cracks that failed to separate the cathode material from the aluminum foil. Therefore, controlling the electrical pulse heating duration to tens of microseconds or less is crucial for achieving separation of the cathode material from the aluminum foil. Only within this time frame can the thermal stress effect from the electrical pulses fully separate the cathode material from the aluminum foil.

3.5. Material characterisation

To ascertain the elemental content in LFP and NCM battery cathode sheets before and after discharge treatments, Inductively Coupled Plasma Optical Emission Spectrometry (ICP-OES) analysis was performed, as shown in Tables 1 and 2. According to Table 1, ICP-OES analysis of the original and 3.0 kV pulse-discharged NCM cathode sheets revealed a drop in impurity aluminum content from 18.3 % to 0.3 % by weight, leading to a recovered cathode material purity of 99.7 %. Table 2 indicates that the original LFP cathode sheets contained 10.4 % aluminum impurities by weight. However, post-treatment with a 3.0 kV pulse discharge, no aluminum impurities were detected in the recovered cathode material, achieving 100 % purity.

Scanning electron microscopy (SEM) was employed to further characterise the microstructure of the original spent LIB cathode materials and the recovered cathode materials. As shown in Fig. 9(a), the NCM cathode material is composed of $Li(Ni_{0.5}Co_{0.2}Mn_{0.3})O_2$ particles mixed with PVDF and acetylene black, with $Li(Ni_{0.5}Co_{0.2}Mn_{0.3})O_2$ particle diameters of approximately 5–10 μm. Fig. 9(c) shows that the $LiFePO_4$ particles in the LFP cathode material are smaller, approximately tens of nanometres in diameter. Fig. 9(a)-(d) indicate that the morphology of NCM and LFP battery cathode materials remains consistent before and after separation, with no significant differences. Maintaining the basic morphology of the cathode material after separation is crucial for the direct regeneration and reuse of cathode materials. A fluffy PVDF binder surrounding the separated cathode particles was also observed. As fluorine (F) is the primary element in PVDF binders, Energy Dispersive X-ray Spectroscopy (EDS) analysis revealed little difference in fluorine content on the surface of cathode materials before and after separation. However, as shown in Fig. 9(e), the aluminum foil surface after separation had very few residual impurities, and the amount of fluorine was significantly reduced compared to that remaining on the surface of the cathode materials.

X-ray Diffraction (XRD) analysis was employed to further characterise the phase of the cathode materials and aluminum foil before and after pulse discharge treatment, as shown in Fig. 10. Fig. 10(a) shows the XRD patterns of the LFP cathode materials before and after pulse discharge treatment. It can be seen that the XRD characteristic diffraction peaks of the cathode materials, both before and after treatment, match those of $LiFePO_4$ in the JCPDF card (No: 00–040–1499). Similarly, the XRD characteristic diffraction peaks of the NCM cathode materials and aluminum foil before and after pulse discharge treatment match those of $Li(Ni_{0.5}Co_{0.2}Mn_{0.3})O_2$ and Al in the JCPDF cards (No: 97–029–1340 and 00–004–0787 respectively).

Furthermore, the primary diffraction peaks of the crystals in the samples before and after separation were completely consistent, with no impurity phases detected. This indicates that the crystal structure and chemical composition of the cathode materials and aluminum foil were not damaged after separation. These results imply that the separation

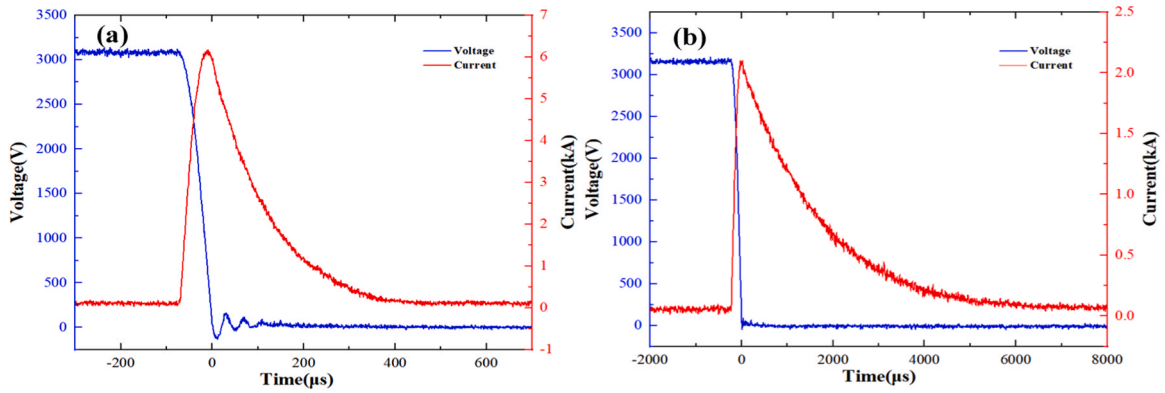

Fig. 7. Current-voltage waveforms of electrical pulses with different pulse widths **(a)** 400 μs; **(b)** 5000 μs.

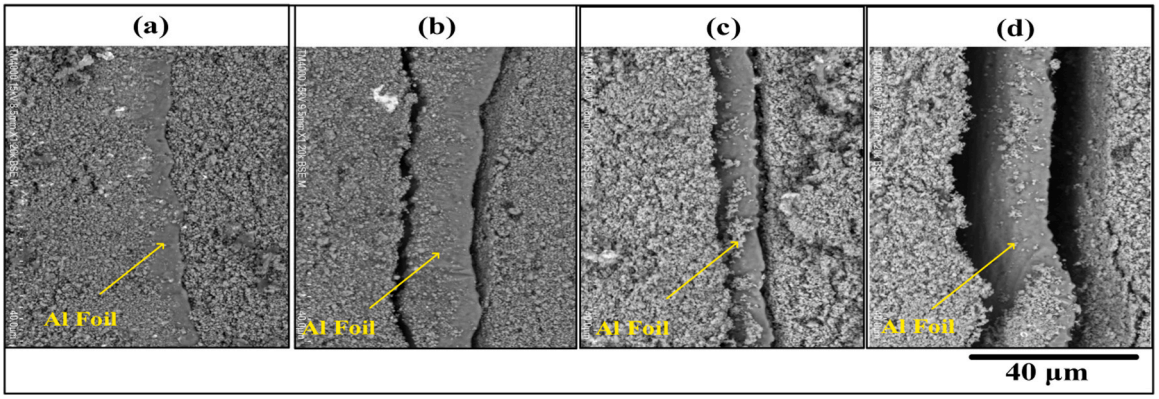

Fig. 8. SEM photographs of cross-sections of LFP battery cathode sheets after different pulse widths of electric pulse treatment **(a)** Original sample; **(b)** Sample treated with 5000 μs pulse width; **(c)** Sample treated with 400 μs pulse width; **(d)** Sample treated with 40 μs pulse width.

Table 1
ICP-OES results of original and 3 kV pulse discharged NCM cathode samples [wt %].

Elements	Ni	Co	Mn	Al	Li	Others
Original NCM	26.0 %	10.8 %	14.1 %	18.3 %	6.4 %	24.4 %
Separated NCM	30.9 %	12.0 %	15.6 %	0.3 %	7.3 %	33.9 %

Table 2
ICP-OES results of original and 3 kV pulse discharged LFP cathode samples [wt %].

Elements	Al	Fe	P	Others
Original LFP	10.4 %	30.4 %	3.9 %	55.3 %
Separated LFP	0 %	31 %	4.23 %	64.77 %

method employed in this study effectively and harmlessly separates the cathode materials and aluminum foil in LFP and NCM batteries. The recovered materials can undergo further hydrometallurgical processing to extract various metal elements and also hold the potential for direct reuse.

3.6. Advantages of the current process

The method proposed in this study was compared with other documented methods for separating cathode materials from aluminum foil in LIBs. Table 3 outlines the treatment conditions, separation efficiency, chemical usage, aluminum foil structural integrity, waste emissions, and types of cathode materials used to evaluate each method.

While the aluminum foil dissolution method and the organic solvent method achieved high recovery efficiencies, they introduced new chemical reagents and led to the production of polluted wastewater or exhaust gases. The mechanical shredding method, being more environmentally friendly, offered lower recovery efficiencies and product purity and failed to maintain the aluminum foil's integrity. Although offering high separation efficiency, the pyrolysis method encountered issues with waste emissions and compromised the structure of the aluminum foil.

Table 3 shows that the method proposed in this study offers

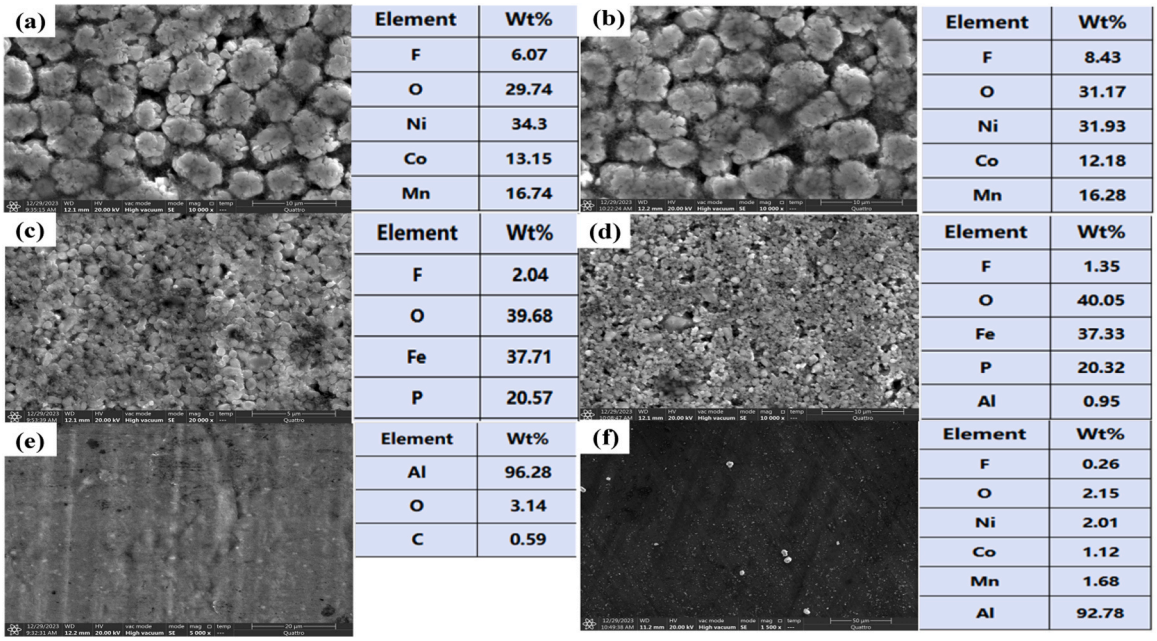

Fig. 9. SEM and EDS results of samples **(a)** original NCM cathode material; **(b)** separated NCM cathode material at a charging voltage of 3.0 kV; **(c)** original LFP cathode material; **(d)** separated LFP cathode material at a charging voltage of 3.0 kV; **(e)** original aluminum foil; **(f)** separated aluminum foil at a charging voltage of 3.0 kV.

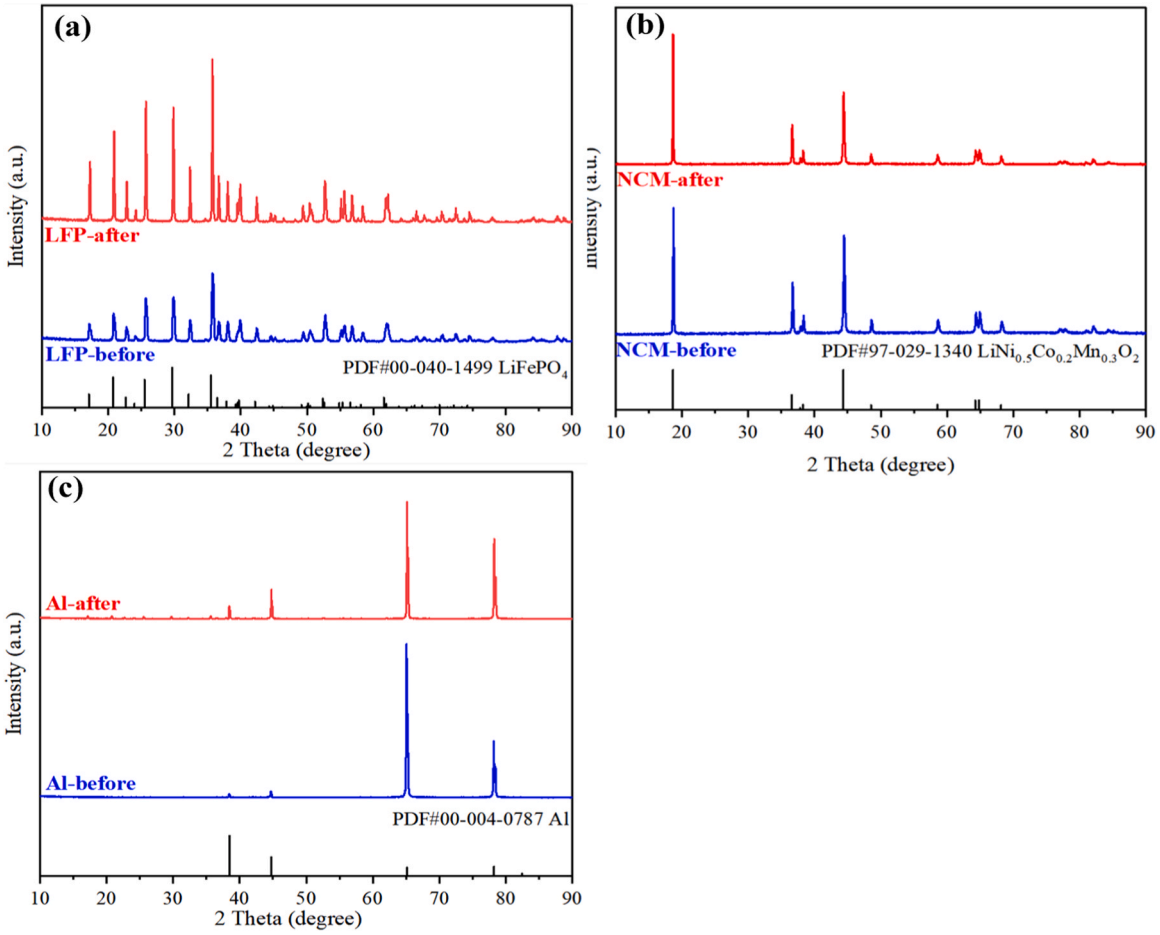

Fig. 10. XRD phase characterisation of samples; **(a)** LFP cathode material before and after separation at a charging voltage of 3.0 kV; **(b)** NCM cathode material before and after separation at a charging voltage of 3.0 kV; **(c)** Aluminum foil before and after separation at a charging voltage of 3.0 kV.

Table 3
Comparison between the existing separation methods of aluminum foil and cathode materials for LIBs and the proposed method.

Method	Treatment condition	Separation efficiency	Use chemicals	Al foil structural integrity	Waste emissions	Cathode materials
Aluminum foil dissolution method [19]	50 °C, 20 g/L NaOH,60 min	99.21 %	Yes	Incomplete	Yes	NCM
Organic solvent method[52]	Cyrene, S/L ratio = 500 g/ L, 100°C, 1 h	100 %	Yes	Complete	Yes	NCM
Organic solvent method[53]	Glycerin,200 °C, 350 r/min, 15 min	95 %	Yes	Complete	Yes	NCM
Mechanical shredding method[54]	Cryogenic ball mill grinding, −38 °C, 5 min	84 %	No	Incomplete	No	NCM
Pyrolysis method[55]	Pyrolysis and crushing, 550 °C and 120 min	94.43 %	No	Incomplete	Yes	LFP
This research	100 μF capacitor discharge at 3.0 kV	99 %	No	Complete	No	NCM/LFP

advantages such as not using chemical reagents, having no wastewater or exhaust emissions, high recovery efficiency (up to 99 % under optimal conditions), and preserving the aluminum foil's structural integrity.

4. Conclusions

The traditional methods of separating cathode materials and aluminum foil for lithium-ion batteries are often energy-intensive and produce significant waste gases and liquids. In this study, an environmentally friendly and highly efficient separation method has been proposed, achieved by using pulsed power technology to instantaneously supply a large amount of Joule heat to the cathode sheet. The mechanism of separation was experimentally explored as follows: the Joule heat resulted in the melting of the PVDF at the interface and potentially induced mild thermal decomposition, significantly diminishing its adhesive properties. Furthermore, thermal stresses were generated at the interface between the cathode materials and aluminum foil, thereby facilitating their separation. The experimental results indicate that both the width and energy of the electrical pulse significantly influence the separation rate, and optimal separation can be achieved by increasing the temperature of the aluminum foil to approximately 750 K in about 40 μs. Different separation behaviors for various battery materials were evidenced by high-speed camera images: LFP cathode materials were separated as a whole, while NCM cathode materials were prone to fracture. At the optimum parameters, the separation rate and product purity reached approximately 99 % and 99.7 %, respectively.

Furthermore, this process successfully preserved the structural integrity of the aluminum foil, as well as the crystal structure and

microstructure of the cathode materials. This method not only facilitates subsequent hydrometallurgical processes for recovering valuable elements but also offers considerable potential for the direct recycling and reuse of both cathode materials and aluminum foil.

Funding

This work was supported by the Natural Science Foundation of Chongqing, China, [grant number CSTB2022NSCQ-MSX1504].

CRediT authorship contribution statement

Yan Mi: Writing – review & editing, Supervision, Project administration, Methodology, Formal analysis. **Yan Zhou:** Supervision, Resources, Methodology, Conceptualization. **Xuzhao Gao:** Writing – review & editing, Software, Formal analysis. **Pengfei Kou:** Writing – original draft, Validation, Methodology, Investigation, Formal analysis, Data curation, Conceptualization. **Hong Wen:** Writing – review & editing, Writing – original draft, Validation. **Chengxiang Li:** Writing – review & editing, Validation, Supervision, Resources, Project administration, Methodology, Funding acquisition, Formal analysis, Conceptualization.

Declaration of Competing Interest

The authors declare the following financial interests/personal relationships which may be considered as potential competing interests: Chengxiang Li reports financial support was provided by Natural Science Foundation of Chongqing, China. If there are other authors, they declare that they have no known competing financial interests or personal relationships that could have appeared to influence the work reported in this paper.

Data Availability

Data will be made available on request.

Acknowledgements

The authors are thankful to Ceshigo Reasearch Serivice (www.ceshigo.com) for providing the testing service.

Appendix A. Supporting information

Supplementary data associated with this article can be found in the online version at doi:10.1016/j.jallcom.2024.174446.

References

[1] Z.P. Cano, D. Banham, S.Y. Ye, A. Hintennach, J. Lu, M. Fowler, Z.W. Chen, Batteries and fuel cells for emerging electric vehicle markets, Nat. Energy *3* (2018) 279–289, https://doi.org/10.1038/s41560-018-0108-1.

[2] Y.X. Wang, B. Liu, Q.Y. Li, S. Cartmell, S. Ferrara, Z.Q.D. Deng, J. Xiao, Lithium and lithium ion batteries for applications in microelectronic devices: a review, J. Power Sources *286* (2015) 330–345, https://doi.org/10.1016/j.jpowsour.2015.03.164.

[3] J. Figgener, P. Stenzel, K.P. Kairies, J. Linssen, D. Haberschusz, O. Wessels, G. Angenendt, M. Robinius, D. Stolten, D.U. Sauer, The development of stationary battery storage systems in Germany - a market review, J. Energy Storage *29* (2020) 20, https://doi.org/10.1016/j.est.2019.101153.

[4] Y. Liang, C.Z. Zhao, H. Yuan, Y. Chen, W. Zhang, J.Q. Huang, D. Yu, Y. Liu, M. M. Titirici, Y.L. Chueh, A review of rechargeable batteries for portable electronic devices, InfoMat *1* (2019) 6–32, https://doi.org/10.1002/inf2.12000.

[5] X. Ma, L. Azhari, Y. Wang, Li-ion battery recycling challenges, Chem *7* (2021) 2843–2847, https://doi.org/10.1016/j.chempr.2021.09.013.

[6] Y. Wang, H. Yin, L. An, An upcoming global challenge: efficient recycling for end-of-life lithium-ion batteries, Glob. Chall. *6* (2022), https://doi.org/10.1002/gch2.202200184.

[7] M. Chen, X. Ma, B. Chen, R. Arsenault, P. Karlson, N. Simon, Y. Wang, Recycling end-of-life electric vehicle lithium-ion batteries, Joule *3* (2019) 2622–2646, https://doi.org/10.1016/j.joule.2019.09.014.

[8] M.M. Wang, C.C. Zhang, F.S. Zhang, An environmental benign process for cobalt and lithium recovery from spent lithium-ion batteries by mechanochemical approach, Waste Manag. *51* (2016) 239–244, https://doi.org/10.1016/j.wasman.2016.03.006.

[9] S.L. Chou, Y.D. Pan, J.Z. Wang, H.K. Liu, S.X. Dou, Small things make a big difference: binder effects on the performance of Li and Na batteries, Phys. Chem. Chem. Phys. *16* (2014) 20347–20359, https://doi.org/10.1039/c4cp02475c.

[10] T. Raj, K. Chandrasekhar, A.N. Kumar, P. Sharma, A. Pandey, M. Jang, B.H. Jeon, S. Varjani, S.H. Kim, Recycling of cathode material from spent lithium-ion batteries: Challenges and future perspectives, J. Hazard. Mater. *429* (2022) 23, https://doi.org/10.1016/j.jhazmat.2022.128312.

[11] H. Al-Shammari, S. Farhad, Heavy liquids for rapid separation of cathode and anode active materials from recycled lithium-ion batteries, Resour. Conserv. Recycl. *174* (2021) 12, https://doi.org/10.1016/j.resconrec.2021.105749.

[12] D.H. Wang, H. Wen, H.J. Chen, Y.J. Yang, H.Y. Liang, Chemical evolution of $LiCoO_2$ and $NaHSO_4{\bullet}H_2O$ mixtures with different mixing ratios during roasting process, Chem. Res. Chin. Univ. *32* (2016) 674–677, https://doi.org/10.1007/s40242-016-5490-2.

[13] K. Liu, F.-S. Zhang, Innovative leaching of cobalt and lithium from spent lithium-ion batteries and simultaneous dechlorination of polyvinyl chloride in subcritical water, J. Hazard. Mater. *316* (2016) 19–25, https://doi.org/10.1016/j.jhazmat.2016.04.080.

[14] N. Chen, J. Qi, X. Du, Y. Wang, W. Zhang, Y.Y. Wang, Y.B. Lu, S.Y. Wang, Recycled $LiCoO_2$ in spent lithium-ion battery as an oxygen evolution electrocatalyst, RSC Adv. *6* (2016) 103541–103545, https://doi.org/10.1039/c6ra23483f.

[15] M.M. Wang, C.C. Zhang, F.S. Zhang, Recycling of spent lithium-ion battery with polyvinyl chloride by mechanochemical process, Waste Manag. *67* (2017) 232–239, https://doi.org/10.1016/j.wasman.2017.05.013.

[16] B.P. Xin, D. Zhang, X. Zhang, Y.T. Xia, F. Wu, S. Chen, L. Li, Bioleaching mechanism of Co and Li from spent lithium-ion battery by the mixed culture of acidophilic sulfur-oxidizing and iron-oxidizing bacteria, Bioresour. Technol. *100* (2009) 6163–6169, https://doi.org/10.1016/j.biortech.2009.06.086.

[17] E.M. Zhen, J.M. Jiang, C. Lv, X.W. Huang, H. Xu, H. Dou, X.G. Zhang, Effects of binder content on low-cost solvent-free electrodes made by dry-spraying manufacturing for lithium-ion batteries, J. Power Sources *515* (2021) 8, https://doi.org/10.1016/j.jpowsour.2021.230644.

[18] L. Li, E.S. Fan, Y.B.A. Guan, X.X. Zhang, Q. Xue, L. Wei, F. Wu, R.J. Chen, Sustainable recovery of cathode materials from spent lithium-ion batteries using lactic acid leaching system, ACS Sustain. Chem. Eng. *5* (2017) 5224–5233, https://doi.org/10.1021/acssuschemeng.7b00571.

[19] C.Y. Li, G.F. Dai, R.Y. Liu, C. Wang, S. Wang, Y. Ju, H.S. Jiang, S.J. Jiao, C.L. Duan, Separation and recovery of nickel cobalt manganese lithium from waste ternary lithium-ion batteries, Sep. Purif. Technol. *306* (2023) 14, https://doi.org/10.1016/j.seppur.2022.122559.

[20] R.J. Zheng, L. Zhao, W.H. Wang, Y.L. Liu, Q.X. Ma, D.Y. Mu, R.H. Li, C.S. Dai, Optimized Li and Fe recovery from spent lithium-ion batteries - a solution-precipitation method, RSC Adv. *6* (2016) 43613–43625, https://doi.org/10.1039/c6ra05477c.

[21] C.K. Lee, K.I. Rhee, Preparation of $LiCoO_2$ from spent lithium-ion batteries, J. Power Sources *109* (2002) 17–21, https://doi.org/10.1016/s0378-7753(02)00037-x.

[22] C. Hanisch, T. Loellhoeffel, J. Diekmann, K.J. Markley, W. Haselrieder, A. Kwade, Recycling of lithium-ion batteries: a novel method to separate coating and foil of electrodes, J. Clean. Prod. *108* (2015) 301–311, https://doi.org/10.1016/j.jclepro.2015.08.026.

[23] M.M. Wang, K. Liu, J.D. Yu, Q.Z. Zhang, Y.Y. Zhang, M. Valix, D.C. Tsang, Challenges in recycling spent lithium-ion batteries: spotlight on polyvinylidene fluoride removal, Glob. Chall. *7* (2023) 18, https://doi.org/10.1002/gch2.202200237.

[24] J. Diekmann, C. Hanisch, L. Froböse, G. Schälicke, T. Loellhoeffel, A.S. Fölster, A. Kwade, Ecological recycling of lithium-ion batteries from electric vehicles with focus on mechanical processes, J. Electrochem. Soc. *164* (2017) A6184–A6191, https://doi.org/10.1149/2.0271701jes.

[25] H.F. Wang, J.S. Liu, X.J. Bai, S. Wang, D. Yang, Y.P. Fu, Y.Q. He, Separation of the cathode materials from the Al foil in spent lithium-ion batteries by cryogenic grinding, Waste Manag. *91* (2019) 89–98, https://doi.org/10.1016/j.wasman.2019.04.058.

[26] M.M. Wang, Q.Y. Tan, L.L. Liu, J.H. Li, Efficient separation of aluminum foil and cathode materials from spent lithium-ion batteries using a low-temperature molten salt, ACS Sustain. Chem. Eng. *7* (2019) 8287–8294, https://doi.org/10.1021/acssuschemeng.8b06694.

[27] M. Wagner, D. Griessl, M. Hiller, A. Kwade, Induction heating as a pre-treatment for the recycling of Li-ion battery cathodes - technical feasibility, J. Clean. Prod. *428* (2023) 9, https://doi.org/10.1016/j.jclepro.2023.139338.

[28] S. Inoue, J. Araki, T. Aoki, S. Maeda, S. Iizasa, M. Takaki, D. Wang, T. Namihira, M. Shigeishi, M. Ohtsu, et al., Coarse aggregate recycling by pulsed discharge inside of concrete, Acta Phys. Pol. A *115* (2009) 1107–1109, https://doi.org/10.12693/APhysPolA.115.1107.

[29] S. Inoue, S. Iizasa, D. Wang, T. Namihira, M. Shigeishi, M. Ohtsu, H. Akiyama, Concrete recycling by pulsed power discharge inside concrete, Int. J. Plasma Environ. Sci. Technol. *6* (2012) 183–188.

[30] S. Lim, Y. Imaizumi, K. Mochidzuki, T. Koita, T. Namihira, C. Tokoro, Recovery of silver from waste crystalline silicon photovoltaic cells by wire explosion, IEEE Trans. Plasma Sci. *49* (2021) 2857–2865, https://doi.org/10.1109/tps.2021.3106307.

[31] C. Duan, Z. Diao, Y. Zhao, W. Huang, Liberation of valuable materials in waste printed circuit boards by high-voltage electrical pulses, Miner. Eng. *70* (2015) 170–177, https://doi.org/10.1016/j.mineng.2014.09.018.
[32] X. Gao, C.X. Xu, H. Yin, X.G. Wang, Q.Z. Song, P.W. Chen, Preparation of graphene by electrical explosion of graphite sticks, Nanoscale *9* (2017) 10639–10646, https://doi.org/10.1039/c7nr01647f.
[33] X. Gao, T. Hiraoka, S. Ohmagari, S. Tanaka, Z.M. Sheng, K.Y. Liu, M. Xu, P. W. Chen, K. Hokamoto, High-efficiency production of large-size few-layer graphene platelets via pulsed discharge of graphite strips, Nanomaterials *9* (2019) 11, https://doi.org/10.3390/nano9121785.
[34] T. Lyon, T. Mütze, U.A. Peuker, Decoating of electrode foils from EOL lithium-ion batteries by electrohydraulic fragmentation, Metals *12* (2022) 17, https://doi.org/10.3390/met12020209.
[35] J. Öhl, D. Horn, J. Zimmermann, R. Stauber, O. Gutfleisch, Efficient process for Li-ion battery recycling via electrohydraulic fragmentation, Proc. Mater. Sci. Forum (2019) 74–78, https://doi.org/10.4028/www.scientific.net/MSF.959.74.
[36] C. Tokoro, S. Lim, K. Teruya, M. Kondo, K. Mochidzuki, T. Namihira, Y. Kikuchi, Separation of cathode particles and aluminum current foil in lithium-ion battery by high-voltage pulsed discharge Part I: experimental investigation, Waste Manag. *125* (2021) 58–66, https://doi.org/10.1016/j.wasman.2021.01.008.
[37] G.W. Zhang, Y.Q. He, Y. Feng, H.F. Wang, T. Zhang, W.N. Xie, X.N. Zhu, Enhancement in liberation of electrode materials derived from spent lithium-ion battery by pyrolysis, J. Clean. Prod. *199* (2018) 62–68, https://doi.org/10.1016/j.jclepro.2018.07.143.
[38] C.Y. Zhang, X.S. Zhu, Y.Z. Xie, J.Y. Wu, X. Huang, H.Y. Xu, P. Feng, Shearing-enhanced mechanical exfoliation with mild-temperature pretreatment for cathode active material recovery from spent LIBs, J. Hazard. Mater. *458* (2023) 15, https://doi.org/10.1016/j.jhazmat.2023.131959.
[39] K. Wang, R.R. Reeber, The perfect crystal, thermal vacancies and the thermal expansion coefficient of aluminium, Philos. Mag. A-Phys. Condens. Matter Struct. Defect Mech. Prop. *80* (2000) 1629–1643, https://doi.org/10.1080/01418610008212140.
[40] K.P. Pramoda, A. Mohamed, I.Y. Phang, T.X. Liu, Crystal transformation and thermomechanical properties of poly(vinylidene fluoride)/clay nanocomposites, Polym. Int. *54* (2005) 226–232, https://doi.org/10.1002/pi.1692.
[41] J.G. Thakare, C. Pandey, M.M. Mahapatra, R.S. Mulik, Thermal barrier coatings-a state of the art review, Met. Mater. Int. *27* (2021) 1947–1968, https://doi.org/10.1007/s12540-020-00705-w.
[42] G. Mehboob, M.J. Liu, T. Xu, S. Hussain, G. Mehboob, A. Tahir, A review on failure mechanism of thermal barrier coatings and strategies to extend their lifetime, Ceram. Int. *46* (2020) 8497–8521, https://doi.org/10.1016/j.ceramint.2019.12.200.
[43] Y.F. Zhang, K.K. Wu, H. Li, S.N. Shen, W. Cao, F. Li, J.Z. Han, Thermal fatigue analysis of gold wire bonding solder joints in MEMS pressure sensors by thermal cycling tests, Microelectron. Reliab. *139* (2022) 7, https://doi.org/10.1016/j.microrel.2022.114829.
[44] L.J. Huang, Z.H. Zhu, H.R. Wu, X. Long, Effect of high-frequency PCB laminate on thermal cycling behavior of electronic packaging structures, Multidiscip. Model. Mater. Struct. *18* (2022) 111–128, https://doi.org/10.1108/mmms-09-2021-0165.
[45] S. Natarajan, M. Akshay, V. Aravindan, Recycling/reuse of current collectors from spent lithium-ion batteries: benefits and issues, Adv. Sustain. Syst. *6* (2022) 8, https://doi.org/10.1002/adsu.202100432.
[46] C.M. Lai, C.H. Su, K.M. Lin, Analysis of the thermal stress and warpage induced by soldering in monocrystalline silicon cells, Appl. Therm. Eng. *55* (2013) 7–16, https://doi.org/10.1016/j.applthermaleng.2013.02.028.
[47] B.W. Nam, J.G. Park, Investigation of wafer warpage induced by multi-layer films, J. Semicond. Technol. Sci. *18* (2018) 7–13, https://doi.org/10.5573/jsts.2018.18.1.007.
[48] L. Sun, K.Q. Qiu, Vacuum pyrolysis and hydrometallurgical process for the recovery of valuable metals from spent lithium-ion batteries, J. Hazard. Mater. *194* (2011) 378–384, https://doi.org/10.1016/j.jhazmat.2011.07.114.
[49] B. Acherjee, A. Kuar, S. Mitra, D. Mitra, Finite element simulation of laser transmission welding of dissimilar materials between polyvinylidene fluoride and titanium, Int. J. Eng. Sci. Technol. *2* (2010) 176-186, https://doi.org/10.4314/IJEST.V2I4.59285.
[50] K. Wang, R.R. Reeber, The perfect crystal, thermal vacancies and the thermal expansion coefficient of aluminium, Philos. Mag. A-Phys. Condens. Matter Struct. Defect Mech. Prop. *80* (2000) 1629–1643, https://doi.org/10.1080/01418610008212140.
[51] K.P. Pramoda, A. Mohamed, I.Y. Phang, T.X. Liu, Crystal transformation and thermomechanical properties of poly(vinylidene fluoride)/clay nanocomposites, Polym. Int. *54* (2005) 226–232, https://doi.org/10.1002/pi.1692.
[52] Y.C. Bai, W.B. Hawley, C.J. Jafta, N. Muralidharan, B.J. Polzin, I. Belharouak, Sustainable recycling of cathode scraps via Cyrene-based separation, Sustain. Mater. Technol. *25* (2020) 7, https://doi.org/10.1016/j.susmat.2020.e00202.
[53] K.H. Gu, J.H. Chang, X.H. Mao, H.B. Zeng, W.Q. Qin, J.W. Han, Efficient separation of cathode materials and Al foils from spent lithium batteries with glycerol heating: a green and unconventional way, J. Clean. Prod. *369* (2022) 9, https://doi.org/10.1016/j.jclepro.2022.133270.
[54] J.S. Liu, X.J. Bai, J. Hao, H.F. Wang, T. Zhang, X. Tang, S. Wang, Y.Q. He, Efficient liberation of electrode materials in spent lithium-ion batteries using a cryogenic ball mill, *J. Environ. Chem. Eng. 9* (2021) 8, https://doi.org/10.1016/j.jece.2021.106017.
[55] X.H. Zhong, W. Liu, J.W. Han, F. Jiao, W.Q. Qin, T. Liu, C.X. Zhao, Pyrolysis and physical separation for the recovery of spent $LiFePO_4$ batteries, Waste Manag. *89* (2019) 83–93, https://doi.org/10.1016/j.wasman.2019.03.068.